Enhanced Hierarchical Control Framework of Microgrids with Efficiency Improvement and Thermal Management

Wang, Yanbo; Liu, Ping; Liu, Dong; Deng, Fujin; Chen, Zhe

Published in:
IEEE Transactions on Energy Conversion

DOI (link to publication from Publisher):
10.1109/TEC.2020.3002670

Publication date:
2021

Document Version
Accepted author manuscript, peer reviewed version

Enhanced Hierarchical Control Framework of Microgrids with Efficiency Improvement and Thermal Management

Yanbo Wang, *Senior Member, IEEE*, Ping Liu, *Senior Member, IEEE*, Dong Liu, *Senior Member, IEEE*, Fujin Deng, *Senior Member*, *IEEE*, Zhe Chen, *Fellow, IEEE*

***Abstract*-This paper presents an enhanced hierarchical control framework of microgrids, as an effective complementary of conventional hierarchical control, to improve operation efficiency and perform thermal management. The enhanced hierarchical control framework is implemented by two control levels. In primary control level, droop control strategy with active thermal management is proposed to perform identical thermal sharing among paralleled inverters. Furthermore, secondary control level is developed to improve operation efficiency and perform thermal management in system-level according to time-varying load profiles, where finite state machine model is adopted to optimize operation number of inverters. In addition, in grid-connected microgrid, resonance phenomena may be caused by time-varying grid impedance. Hence, resonance mitigation strategy of microgrid is developed in the secondary control level, and small signal model of grid-connected microgrid is established to investigate the resonance phenomenon. Simulation and experimental results show that the proposed hierarchical control framework is able to perform active thermal management, improve operation efficiency, and mitigate harmonic resonance in either autonomous mode or grid-connected mode. The proposed hierarchical control framework is an enhanced complementary for conventional hierarchical control of microgrids.**

***Index Terms*—Enhanced hierarchical control, thermal stress, droop control, efficiency, active thermal control, resonance mitigation, finite state machine.**

I. Introduction

With the increasing penetration of renewable energies, small-scale distributed power systems such as microgrids and active distribution networks [1]-[2] are becoming attractive solutions to integrate various distributed energy sources, energy storage devices and local loads [1], which is able to improve control flexibilities and system reliability.

Energy management is an essential aspect for microgrid operation. Hierarchical control strategies have been frequently developed in droop-controlled microgrids to guarantee the steady-state and dynamic performance of power control [2]-[8] in different control levels. Hierarchical control structure is able to ensure flexibility and expansibility of power control in the presence of additional Distributed Generators (DG), which can support plug and play operation of distributed generators. A three-level hierarchical control structure of droop-controlled microgrids is presented in [3], which consists of primary control level, secondary control level and tertiary control level. A hierarchical control system is developed to manage operation performance with consideration of economic aspects [4]. A robust hierarchical control system of active distribution systems is proposed in [5] to provide disturbance rejection performance against voltage disturbances and power angle fluctuation. The main tasks of existing hierarchical control structure [2]-[8] are summarized as follows.

(1) ***Primary Level***: The aim of primary control is to perform proportional power sharing among paralleled inverters without using critical communication facilities.

(2) ***Secondary Level***: The responsibility of secondary control is to restore frequency and voltage deviations caused by primary control. Also, synchronous control with utility grid is performed in this level.

(3) ***Tertiary Level***: The tertiary control commonly performs power flow control between microgrids and grid. In grid-connected microgrid, the power flow can be controlled by adjusting the frequency and amplitude of the voltage inside the microgrid. In addition, auxiliary service strategies such as smooth transition and fault monitoring can be performed in the tertiary level.

Microgirds are often adopted to provide reliable electricity services for safe-critical systems [9]-[10], where reliability is one of essential concerns. In fact, operating temperatures of power devices have significant impacts on long-term reliability of power electronic system, where over-temperature and temperature fluctuations caused by power loss can result in power devices failures [10]. In practical operation of microgrids, unequal thermal sharing among paralleled inverters tend to mitigate long-term lifetime of microgrids due to difference of inverter electro-thermal parameters [9]-[10]. Active thermal control strategies have been proposed to increase average lifetime cycle of inverters [10]-[12]. The general principle of active thermal control is to vary one or more temperature-related control variables of the system to reduce the thermal cyclying of power semiconductors during nominal operation. The temperature-related control variables commonly include the switching frequency [13], modulation method [14], DC-link voltage [15], output current limit [16], and parameters in active gate control [17]. However, the active thermal control also exists limitations, which may lead to the decrease of the overall system efficiency, performance deterioration, or increased control complexity with additional thermal control loops [18]-[19]. Active thermal control by regulating the current control limit benefits long-term lifetime

This article has been accepted for publication in a future issue of this journal, but has not been fully edited. Content may change prior to final publication. Citation information: DOI 10.1109/TEC.2020.3002670, IEEE Transactions on Energy Conversion

of power converter, but implies a restriction of system performance.

To improve long-term reliability of power converters, an active thermal control-based current sharing scheme for paralleled inverters is proposed in [6], where the effect of parameters variation on temperature is investigated and load current is redistributed among paralleled inverters according to their temperature difference. In case of paralleled power converters, power routing can be used to share the total power intelligently between the converters to reduce or balance the thermal stress in a modular structure, which is effective to achieve active thermal control for reliability improvement of converters [13].

In microgrids, the efforts toward reliability enhancement are slightly performed. Existing hierarchical control strategies mainly focus on power control in microgrids, which fails to enhance system long-term reliability. A hybrid control architecture is presented in [20] to implement system thermal management. A lifetime-oriented droop control strategy is proposed in [9] to perform equal thermal sharing. However, the aforementioned work fails to implement overall thermal management and efficiency improvement in system-level.

Furthermore, operation efficiency of microgrid is another important concern. In fact, microgrid efficiency is affected due to different load profiles. The aspect about efficiency improvement of microgrids has been paid very limited attention. A power sharing and power-shifting strategy is presented in [21] to improve system efficiency of paralleled inverters. A distributed optimization method based on dynamic consensus algorithm is presented in [22] to improve operation efficiency of droop-controlled DC microgrids. However, high bandwidth communication channels are required to support the distributed control strategy. An adaptive droop control strategy is developed in [23]-[24] to improve operation efficiency of microgrids under different load profiles, where efficiency model of microgrid is first established to analyze time-varying characteristic of efficiency under different load profiles, and optimum solution of efficiency model is derived by lagrange multiplier method. However, the proposed control method fails to deal with thermal issue of paralleled inverters.

Additionally, microgrids can be operated in grid-connected mode to transmit power to utility grid according to commands of power system. Resonance phenomena can be triggered due to time-varying grid impedance, which can increase thermal stress of power devices, and weaken long-term reliability of microgrids [25]-[28]. However, existing hierarchical control strategies fails to deal with the resonance phenomena caused by time-varying grid impedance.

To improve operation efficiency and reliability of microgrids, an enhanced hierarchical control framework of microgrid was proposed in our previous conference version [29]. As an extension, this paper developes a comprehensive hierarchical control framework of microgrids with efficiency improvement and thermal management, which consists of primary control level and secondary control level. The motivation of this work is to develop an enhanced hierarchical control framework of microgrids, which is able to implement efficiency improvement, thermal management and resonance mitigation, so that the comprehensive performance can be improved.

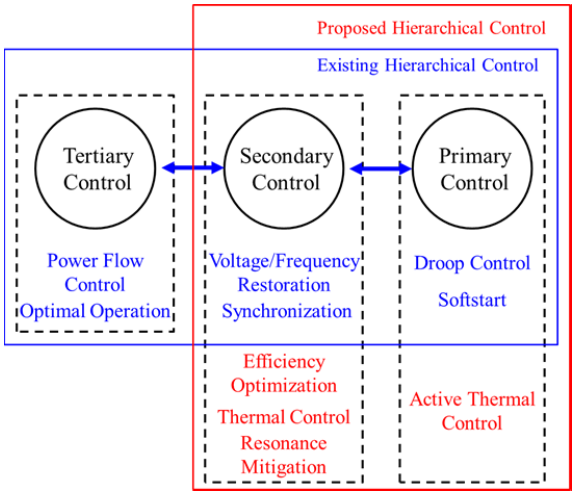

Fig. 1. Hierarchical control structure of droop-controlled microgrids.

Fig. 1 shows the relationship between the proposed hierarchical control and conventional hierarchical control. In primary control level, thermal management-oriented droop control is proposed to perform active thermal sharing among paralleled inverters. Secondary controller is developed to optimize system efficiency under different load profiles and perform thermal control in system-level. In addition, resonance mitigation capability is developed to mitigate harmonic resonance phenomena in grid-connected mode by means of finite state machine. The proposed hierarchical control framework is able to improve operation efficiency and implement thermal management for microgrids. Further, the the proposed control is compatible with tertiary control to enable optimal power flow control as an effective complementary of conventional hierarchical control framework.

The rest of this paper is organized as follows. In Section II, electro-thermal model of inverter are established to estimate thermal dissipation of microgrid. In Section III, an enhanced hierarchical control structure is proposed, where the principle and implementation details of it are given. Simulation and experimental results are given to validate the proposed hierarchical control strategy in Section IV and Section V. Conclusions are drawn in Section VI.

II. Electro-thermal Model of Inverter

Electro-thermal model of inverter are first established to estimate thermal dissipation, which will be applied in primary and secondary control level.

Power loss of power devices and diode can be calculated [9],[29]-[31] as (1) and (2).

$$P_{loss\_PD} = P_{con\_PD} + P_{sw\_PD} \tag{1}$$

$$P_{loss\_Diode} = P_{con\_diode} + P_{rec\_diode} \tag{2}$$

where average conduction losses of power device (P_{con_PD}) and diode (P_{con_diode}) during a fundamental period may be represented as (3) and (4) [29]-[31].

$$P_{con\_PD} = \frac{1}{2}\left(V_{ce0}\frac{I_m}{\pi} + r\frac{I_m^2}{4}\right) + m\cos\phi\left(V_{ce0}\frac{I_m}{8} + \frac{1}{3\pi}rI_m^2\right) \tag{3}$$

This article has been accepted for publication in a future issue of this journal, but has not been fully edited. Content may change prior to final publication. Citation information: DOI 10.1109/TEC.2020.3002670, IEEE Transactions on Energy Conversion

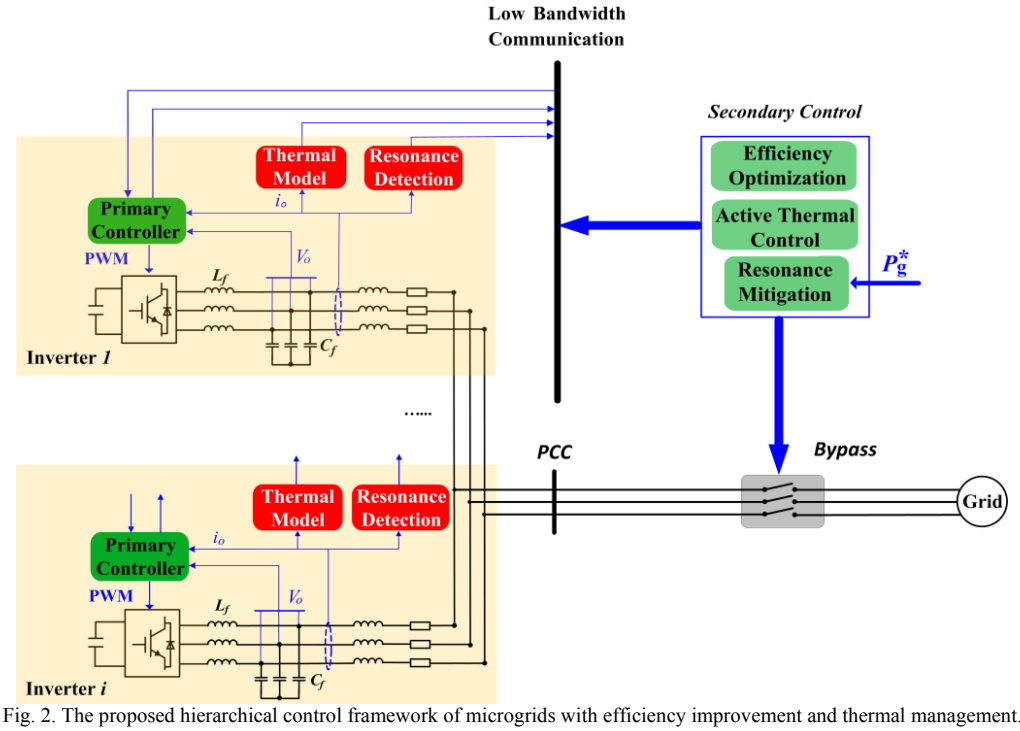

Fig. 2. The proposed hierarchical control framework of microgrids with efficiency improvement and thermal management.

$$P_{con\_Diode} = \frac{1}{2}(V_{T0}\frac{I_m}{\pi} + r_d\frac{I_m^{\ 2}}{4}) - m\cos\phi\cdot(V_{T0}\frac{I_m}{8} + \frac{1}{3\pi}r_d I_m^{\ 2}) \quad (4)$$

where V_{ce0} and V_{T0} are constant voltage drop of power device and diode, r and r_d are current magnitude dependent voltage in output characteristic of on-state voltage and collector current for power device and diode [29]-[31]. ϕ is the phase angle between voltage and current. ω is fundamental angle frequency. I_m is amplitude of load current. m is modulation index related with AC voltage amplitude to DC-link voltage. The average switching losses of power device during a fundamental period (T_0) is given [31] as (5).

$$P_{sw\_PD} = \frac{1}{T_0}\sum_1^n E_{sw}(i) \quad (5)$$

E_{sw} is the sum of turn-on and turn-off energy dissipation, which is given as (6).

$$E_{sw}(i) = (E_{on}(I_{nom}, V_{nom}) + E_{off}(I_{nom}, V_{nom}))\frac{i}{I_{nom}}\cdot\frac{V_{dc}}{V_{nom}} \quad (6)$$

The recovery loss of diode can be calculated [31] as (7).

$$P_{rec\_diode} = \frac{1}{\pi}f_{sw} * E_{rec}(I_{nom}) * (0.45\frac{i}{I_{nom}} + 0.55) * \frac{V_{dc}}{V_{nom}} \quad (7)$$

E_{on} and E_{off} are measured turn-on and turn-off energy dissipation of power device at each switching pulse from datasheet. i is phase leg current. I_{nom} and V_{nom} are nominal current and voltage of power device. V_{dc} is DC-link voltage. f_{sw} is switching frequency. E_{rec} is recovery loss of diode.

Junction temperature of power device can be estimated by RC equivalent thermal models without direct measurements [10], [30]. In this work, equivalent thermal model is established to predict temperature of power devices, where only steady-state junction temperature is estimated to implement steady-state active thermal control. Thermal resistance is a critical parameter to determine the thermal behavior of power devices. Fig. 3 shows thermal resistance chain of power devices applied in this work [30], where each current source represents the thermal power losses of power device. R_{thJC_PD} and R_{thJC_D} are thermal resistance of power device and diode from junction to case. R_{thCH_PD} and R_{thCH_D} are thermal resistance of power device and diode from case to heat sink. R_{thHA} are the thermal resistance of heatsink to ambient environment.

The junction temperature of power device and diode can be derived from the equivalent thermal model [30], [32] as shown in Fig. 3 as (8) and (9).

$$T_{jun\_PD} = P_{loss\_PD}\cdot(R_{thJC\_PD} + R_{thCH\_PD}) + T_H \quad (8)$$

$$T_{jun\_D} = P_{loss\_D}\cdot(R_{thJC\_D} + R_{thCH\_D}) + T_H \quad (9)$$

where T_{jun_PD} and T_{jun_D} are junction temperature of power device and diode, T_a is the ambient temperature. And T_H=(P_{loss_PD}+P_{loss_D})·R_{thHA}+T_a.

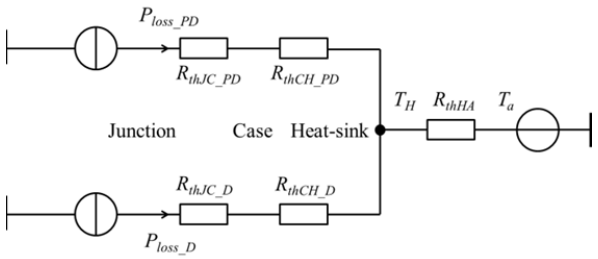

Fig. 3. Equivalent thermal model of semiconductor power device [32].

III. The Proposed Enhanced Hierarchical Control Framework

In this section, the principle of the proposed enhanced hierarchical control framework is developed, where the implementation procedures of primary control level and secondary control level are given. Fig. 2 shows the diagram of the proposed enhanced hierarchical control framework of

This article has been accepted for publication in a future issue of this journal, but has not been fully edited. Content may change prior to final publication. Citation information: DOI 10.1109/TEC.2020.3002670, IEEE Transactions on Energy Conversion

microgrids with efficiency improvement and thermal management. Junction temperature estimation model of power devices is first established to predict thermal characteristics, and two-level control framework is formulated, respectively.

A. Primary control level: thermal sharing

Primary control level is developed to perform thermal stress sharing among paralleled inverters. Temperature-current relationship of different inverters is first obtained by combining (8)-(9) and parameters in Table I [33]-[34] as shown in Fig. 4, where inverters have different temperature-current characteristics due to differences of power devices. To make assure that the power devices can be operated within a desirable operation temperature range, the typical heat sink WA-T264-101E is applied in this work, where the thermal resistance parameter from heat sink to ambient (R_{thHA}) is given in Table I according to datasheet of heat sink [35].

Mathematical representation of temperature-current relationship is obtained from Fig. 4 by the least square fitting as (10)-(11).

$$T_{PD}(I_c) = a_1 I_c^{\,2} + b_1 I_c + c_1 \tag{10}$$

$$T_{Diode}(I_c) = a_2 I_c^{\,2} + b_2 I_c + c_2 \tag{11}$$

where $T_{PD}(I_c)$ and $T_{Diode}(I_c)$ are current-dependent junction temperature of power device and diode. $a_1, b_1, c_1, a_2, b_2, c_2$ are coefficients of fitted equations, which can be obtained according to Fig. 4. The primary control strategy is validated in a microgrid with 4 inverters.

TABLE I
PARAMETERS APPLIED IN ELECTRO-THERMAL MODEL [33]-[34]

Inverter 1/Inverter 3		Inverter 2/Inverter 4	
Power device	FP10R06KL4	Power device	FS6R06VE3B2
$R_{\text{thJC\_PD}}$	1.6 K/w	$R_{\text{thJC\_PD}}$	3.3 K/w
$R_{\text{thCH\_PD}}$	0.6 K/w	$R_{\text{thCH\_PD}}$	1.3 K/w
$R_{\text{thJC\_D}}$	3.5 K/w	$R_{\text{thJC\_D}}$	4.5 K/w
$R_{\text{thCH\_D}}$	1.1 K/w	$R_{\text{thCH\_D}}$	2.1 K/w
R_{thHA}	11 K/w		
Voltage (Base value)	110 V	Temperature (Base value)	75 °C
Current (Base value)	12 A	Frequency (Base value)	50 Hz

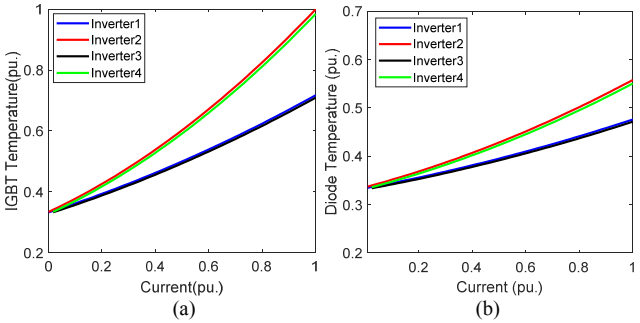

Fig. 4. Temperature-current relationship of 4 inverters. (a) Current-dependent power device junction temperature. (b) Current-dependent diode junction temperature.

New active power-frequency (*P-f*) and reactive power-voltage (Q-*V*) droop relationships with consideration of active thermal control are formulated by combining temperature-current relationship (10)-(11) and conventional droop curves as (12)-(14).

$$f_x^* = f_{\max} - \frac{f_{\max} - f_{\min}}{P_{\max}(T_{PD\_\max})} \times T_{PD}\left(\frac{P_x}{V_{nom}}\right) \tag{12}$$

$$V_{ox}^* = V_{\max} - \frac{V_{\max} - V_{\min}}{Q_{\max}(T_{PD\_\max})} \times T_{PD}\left(\frac{Q_x}{V_{nom}}\right) \tag{13}$$

$$or \qquad V_{ox}^* = V_{\max} - \frac{V_{\max} - V_{\min}}{Q_{\max}(T_{Diode\_\max})} \times T_{Diode}\left(\frac{Q_x}{V_{nom}}\right) \tag{14}$$

(x=1,2,3,4) is x-th inverter in microgrid. The proposed *P-f* droop curves (12) and *Q-V* droop curves (13) are shown in Fig.5. In the droop-controlled microgrid, the DG inverters are regarded as dispatchable resources or renewable energy resources equipped with energy storage devices [2]-[8] to ensure propotional power sharing among paralleled inverters. In this work, the power sharing among paralleled inverters is perfomed according to the temperature-dependent power ratings. The inverter with lower temperature will generate higher powers. Then, the thermal stress is redistributed, which thus achieves equal thermal distributions among paralleled inverters.

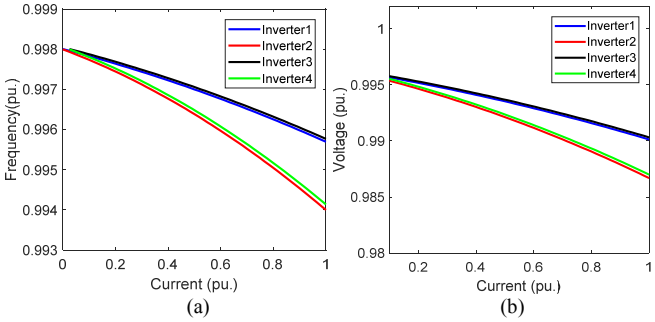

Fig. 5. The proposed lifetime-oriented droop control. (a) The temperature-dependent *P-f* droop curve. (b) The temperature-dependent *Q-V* droop curve.

To futher analyze the effect of thermal stress on long-term lifetime of power devices, the extended Coffin-Manson lifetime model [36] is employed to explain the relationship between power device lifetime and junction temperature as (15).

$$N_f = \alpha \cdot (\Delta T_j)^{-n} \cdot \exp\left(\frac{E_a}{k_B \cdot T_{jmean}}\right) \tag{15}$$

where N_f is the number of cycles to failure, α = 302500, n = 5.039, $E_a = 9.891\times10^{-20}$ J, k_B is Boltzmann constant, ΔT_j is the junction temperature swing (thermal cycling) and T_{jmean} is the mean junction temperature (thermal loading) of the power device. Then, the lifetime of microgrid under proposed control strategy can be predicted according to the extended Coffin-Manson lifetime model [36]. In this work, the proposed control framework is implemented by redistributing the power among paralleled inverters according to different load profiles to regulate the mean junction temperature (T_{jmean}), so that the efficiency optimization and thermal management can be implemented simultaneously.

B. Secondary Control Level: Active thermal management and resonance mitigation

The responsibility of secondary control level is to optimize operation efficiency of microgrid under different load profiles. Fig. 6 shows the well-established efficiency curves of single and paralleled inverters [20].

This article has been accepted for publication in a future issue of this journal, but has not been fully edited. Content may change prior to final publication. Citation information: DOI 10.1109/TEC.2020.3002670, IEEE Transactions on Energy Conversion

It can be seen that the efficiency of paralleled inverters is lower than that of single inverter when load power is lower than 50% of inverter rated power. Hence, the optimum efficiency points are time-varying as variation of load conditions. In second control level, operating points of microgrid are dynamically shifted by optimizing operation number of inverters to improve operation efficiency according to load profiles and thermal distribution status. Specific inverters are controlled to generate higher power and the rest of inverters are reactivated under light-load condition. On the other hand, once inverter temperature is higher than critical value, the more inverters will be activated to share loads power, where temperature of power devices is estimated according to thermal model established in Section III. A.

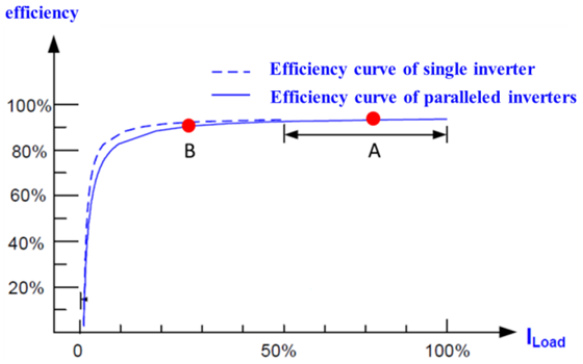

Fig. 6. Efficiency curves of power converters [20].

To implement dynamic shift of operating points, finite state machine model [37] is adopted to model secondary controller, where the control signals as Boolean variables can be transmitted by low bandwidth communication. The model defines a finite set of states as well as how the system is shifted from one state to another when certain conditions happen. Fig. 7 shows the finite state machine-based secondary control strategy in islanded microgrids, where two operation modes including efficiency optimization and active thermal control are performed to track optimum operation points. Fig.7(a) shows the interaction relationship of primary control level and secondary control level. Fig. 7(b) shows possible transitions between different states, where dynamics of finite state machine are defined and each state can be shifted by a Boolean condition. In this work, the control bandwidth of secondary controller is designed as 10Hz. With the assumption that the microgrid consists of 4 inverters, it thus can be controlled at 4 operation states. S_x (x=1,2,3,4) indicates operation status, where x is operation number of inverters under each state.

Boolean logical variables are first defined here. θ_x is defined as switch on/off status of inverter. T_x indicates thermal operation status of inverter. δ_x indicates load status of DG inverter. Two operation modes are explained as following.

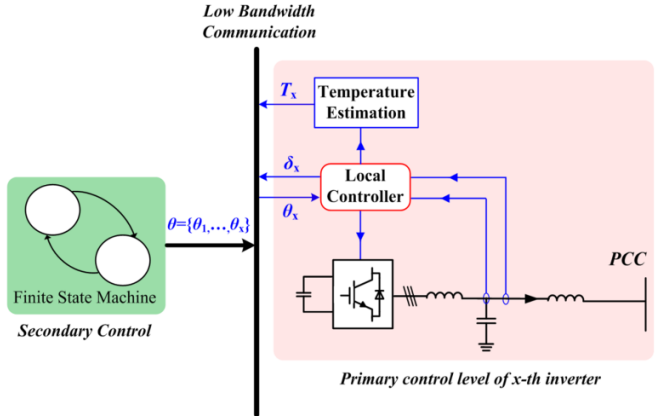

(a)

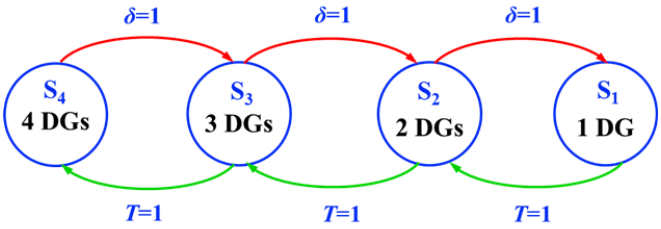

(b)

Fig. 7 The finite state machine-based secondary control strategy

(1) Active thermal management

The trigger condition is defined by discrete logic variables as (16) and (17).

$$[T_e > T_c] \rightarrow [T_x = 1] \tag{16}$$

$$T = T_1 \vee T_2 \vee \cdots \vee T_x \tag{17}$$

T_e is estimated operation temperature of inverter according to electro-thermal model. T_c is defined as critical temperature to trigger state transition. In this work, T_c is defined as 120°C. Once T_e is higher than T_c, thermal status of each inverter T_x will be switched to 1. T is thermal indicator of microgird, where it will be switched as 1 to trigger secondary controller if thermal status of any inverters is switched to 1. Then, the microgrid will be shifted into operating point B as shown in Fig. 6. Then, the rest of inverters are sequentially activated to share load power so that thermal stresses are redistributed.

As illustrated in Fig. 6, efficiency of paralleled inverters is not optimum if system is operated under light-load condition (point B) where output power is lower than 50% of rated power. To improve system efficiency, the number of inverters is decreased to capture optimum operating point. The secondary control strategy will move it into operating point A by state transitions. The trigger condition is defined as (18) and (19).

$$[P_x < 50\% P_{rated}] \rightarrow [\delta_x = 1] \tag{18}$$

$$\delta = \delta_1 \vee \delta_2 \vee \cdots \vee \delta_x \tag{19}$$

where P_x is output power of i-th inverter. P_{rated} is rated power of inverter. It is defined that microgrid is under light-load condition if P_x is lower than 50% P_{rated}, then load status variable δ_x is switched to 1, and secondary controller is enabled to reduce operation number of inverters for efficiency improvement. The logical truth table indicating operation status of inverters is given in Table II.

This article has been accepted for publication in a future issue of this journal, but has not been fully edited. Content may change prior to final publication. Citation information: DOI 10.1109/TEC.2020.3002670, IEEE Transactions on Energy Conversion

TABLE II
LOGICAL TRUTH TABLE INDICATING OPERATION STATUS

	θ_1	θ_2	θ_3	θ_4
S_1	1	1	1	1
S_2	1	1	1	0
S_3	1	1	0	0
S_4	1	0	0	0

(2) Resonance mitigation

When microgrid is operated in grid-connected mode, resonance phenomenon can be caused due to time-varying grid impedance. In grid-connected mode, resonance mitigation capability is developed in secondary control level. Resonance detection of inverter current is implemented by measuring amplitude of output current using Fast Fourier Transformation (FFT). The resonance detection block is able to identify whether the current magnitude in present control period is increased compared with the threshold.

Small signal model of grid-connected microgrid is first established to analyze the resonance behaviors. Fig. 8(a) shows the diagram of individual inverter, and Fig. 8(b) shows the equivalent circuit of grid-connected microgrid with 4 inverters, where i_{ox} (x=1,2,3,4) is output current of x-th inverter, i_g is grid-injected current of paralleled inverters, V_{pcc} is voltage at point of common coupling. L_g and R_g are equivalent grid impedance and resistor.

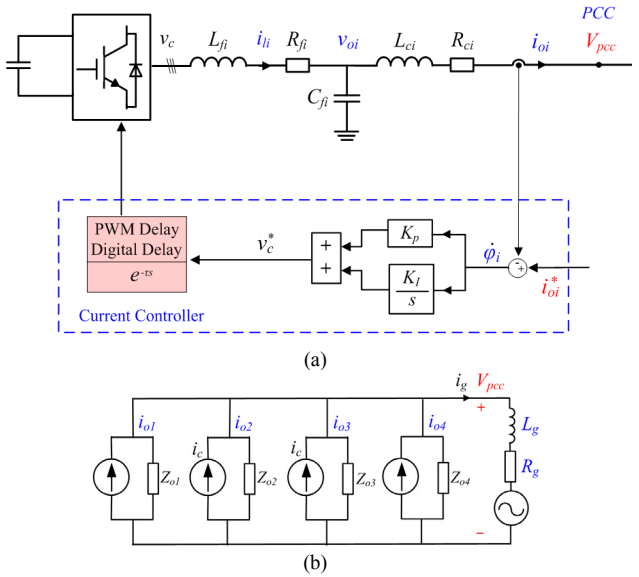

Fig. 8 The diagram of grid-connected microgrid. (a) The diagram of individual inverter with controller. (b) The equivalent circuit of grid-connected microgrid.

State-space equation of individual inverter considering *LCL* filter, current controller and time delay of digital controller can be established as (20) and (21).

$$\dot{x}_{invi} = A_{invi}x_{invi} + B_{invi}u_{invi} \tag{20}$$

$$y_{invi} = C_{invi}x_{invi} \tag{21}$$

where $x_{invi} = [i_{li}, v_{oi}, i_{oi}, \phi_i, x_d](i = 1,2,3,4)$, $u_{invi} = [i_{oi}^*, V_{pcc}]$, $y_{invi} = [i_{oi}]$. The i_{li} and i_{oi} are converter-side current and grid-side current of inverter as shown in Fig. 8(a). v_{oi} is output voltage of inverter. φ_i is state variables of current controller. x_d are state variables of equivalent delay plant of digital controller. A_{invi}, B_{invi}, C_{invi} are parameter matrices. The detailed parameters and derivation process can be seen in [28].

Dynamic equation of grid current i_g can be derived as (22).

$$\dot{i}_g = -\frac{R_g}{L_g}i_g + \frac{1}{L_g}V_{pcc} \tag{22}$$

The overall state-space model is established by combining (9)-(10) and (13) as (23).

$$\dot{x}_{sys} = A_{sys}x_{sys} + B_{sys}V_{pcc} \tag{23}$$

where $x_{sys} = [x_{invl}, x_{inv2}, x_{inv3}, x_{inv4}, i_g]^T$, $A_{sys} = diag(A_{invl}, A_{inv2}, A_{inv2}, A_{inv4}, -\frac{R_g}{L_g})$ is the diagonal state matrix, $B_{sys} = \left[B_{invl}, B_{inv2}, B_{inv3}, B_{inv4}, \frac{1}{L_g}\right]^T$

To establish a simplified state-space model, a virtual resistor (R_n) is introduced to define PCC voltage [28] as (24).

$$V_{pcc} = R_n(i_{o1} + i_{o2} + i_{o3} + i_{o4} - i_g) \tag{24}$$

The PCC voltage equation may be rewritten as (25) by combining (21) and (24).

$$V_{pcc} = Nx_{sys} \tag{25}$$

where $N = R_n[C_{invl}, C_{inv2}, C_{inv3}, C_{inv4}, -1]$.

The small signal model of microgrid can be established by combining (23) and (25) as (26)

$$\dot{x}_{sys} = F_{sys}x_{sys} \tag{26}$$

where $F_{sys} = A_{sys} + B_{sys}N$ is state matrix of overall system.

The eigenvalue trace of state matrix (F_{sys}) indicates the oscillation characteristic and damping characteristic of the overall system. Fig. 9(a) shows eigenvalue trace of microgrid as increase of grid impedance. And Fig. 9(b) shows the eigenvalue trace of microgrid as decrease of inverter number. The small signal analysis shows that operation number of inverter contributes to output impedance of microgrid and has significant effects on small signal stability of microgrid.

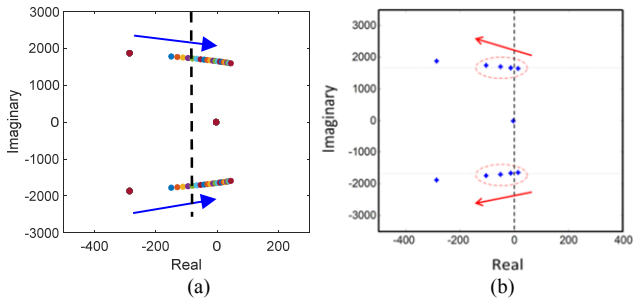

Fig. 9. Eigenvalue trace of microgrid. (a) Eigenvalue trace as increase of grid impedance. (b) Eigenvalue trace as decrease of inverter number.

Resonance mitigation capability is developed in secondary control level to mitigate resonance phenomena according to small signal analysis from Fig. 9. Fig. 10 shows operation principle of the proposed secondary control strategy. Fig.10(a) shows the interaction relationship of secondary control and primary control level, and Fig. 10(b) shows state transition procedure triggered by secondary controller.

This article has been accepted for publication in a future issue of this journal, but has not been fully edited. Content may change prior to final publication. Citation information: DOI 10.1109/TEC.2020.3002670, IEEE Transactions on Energy Conversion

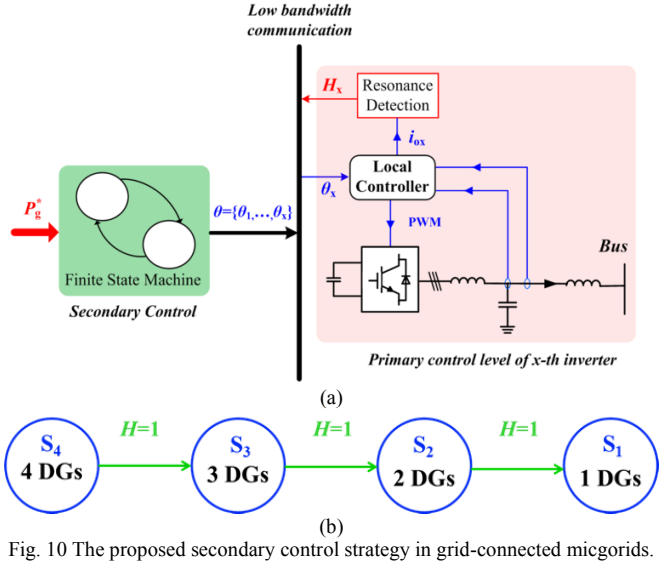

Fig. 10 The proposed secondary control strategy in grid-connected micgorids.

Once the measured THD value from resonance detection block is higher than critical value, system status can be shifted to other states. The trigger condition is defined as (27) and (28)

$$[H_M > H_c] \rightarrow [H_x = 1] \tag{27}$$

$$H = H_1 \vee H_2 \vee \cdots \vee H_x \tag{28}$$

where H_M is measured THD value, H_c is threshold to trigger secondary controller and H_x is Boolean variable that indicates harmonic status of each inverter.

Then, power reference command is updated to assign output power of each inverter as (29)

$$P_i^* = \frac{P_g^*}{n - (H_1 + H_2 + \ldots + H_x)} \tag{29}$$

where P_g^* is total power command from grid. n is total number of inverters in microgrid.

IV. Simulation Verification

To validate effectiveness of the proposed hierarchical control strategy, simulations in MALAB with PLECS blockset and Stateflow blockset are performed in a scaled-down microgrid. The circuit diagram of microgrid with 4 inverters is shown in Fig. 2. The system parameters applied in simulation are given in Table I and Table IV.

Case I Proposed primary control strategy

Fig. 11 shows the simulation results of paralleled inverters under conventional droop control method. It can be seen from Fig. 11(b) that thermal stress is unequally distributed due to difference of electro-thermal parameters for 4 inverters, even if equal power sharing can be achieved.

Fig. 12 shows the simulation results of microgrid with the proposed thermal management-oriented droop controller. It can be seen from Fig. 12(b) that the proposed primary control strategy is able to share automatically thermal stress by regulating active powers of inverters, so that the thermal dissipation can be equally distributed between inverter 1 and inverter 2. Fig. 13 shows simulation results of paralleled inverters when reactive power loads is increased. It can be seen from Fig. 13(b) that the droop controller is able to equally redistribute thermal stress between paralleled inverters by regulating output reactive powers.

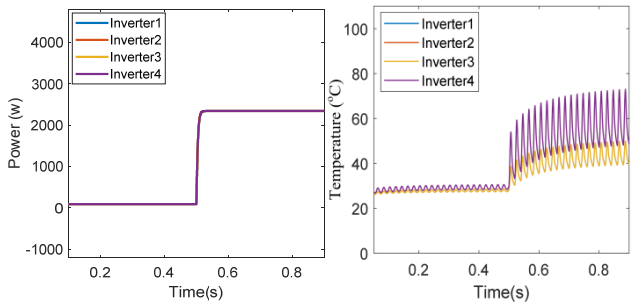

Fig. 11. Simulated results of 4 paralleled inverters with parameters shown in TableI. (a) Active power sharing of inverters. (b) Power device junction temperature of inverters.

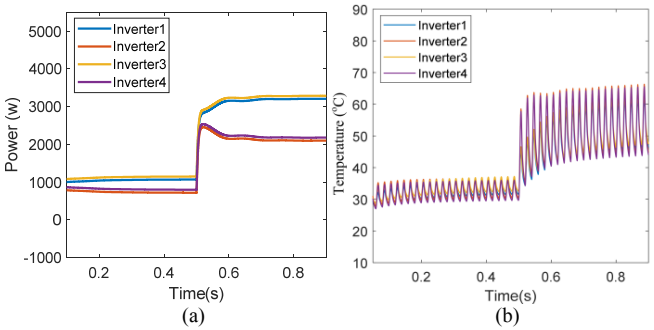

Fig. 12 Simulated results of 4 paralleled inverters with parameters shown in TableI under the proposed lifetime-oriented droop controller. (a) Active power sharing of inverters. (b) Power device average junction temperature of inverters.

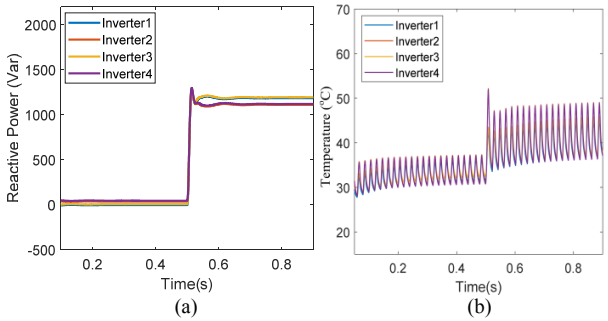

Fig. 13 Simulated results of 4 paralleled inverters with parameters shown in TableI. (a) Reactive power sharing of inverters. (b) Power device average junction temperature of inverters.

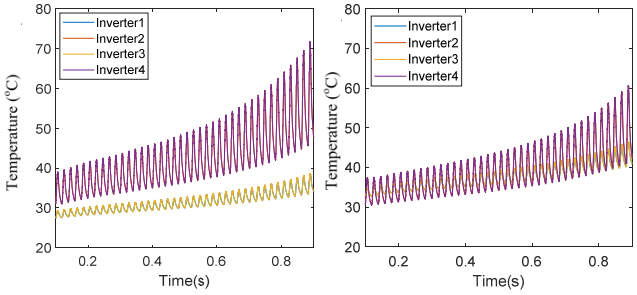

Fig. 14. Simulated results of 4 paralleled inverters with parameters shown in TableI. Power device junction temperature of inverters for gradual change of the load without the proposed primary control. (d) Power device junction temperature of inverters for gradual change of the load with the proposed primary control.

This article has been accepted for publication in a future issue of this journal, but has not been fully edited. Content may change prior to final publication. Citation information: DOI 10.1109/TEC.2020.3002670, IEEE Transactions on Energy Conversion

Fig. 14 shows the simulation results of 4 paralleled inverters without and with the proposed primary control for gradual change of the load. It can be seen that the proposed primary control strategy is able to share automatically thermal stress in the presence of gradual change of the load.

To further evaluate the lifetime of microgrid, a comparison analysis of junction temperatures and the number of cycles to failure is given in Table III according to Fig. 11-13.

TABLE III

COMPARISON JUNCTION TEMPERATURES AND N_F RESULTS

	Conventional droop control		Proposed droop control	
Inverter	Inverter 1/3	Inverter 2/4	Active Power (Inverter 1-4)	Reactive Power (Inverter 1-4)
T_{jmean} (°C)	42	60	53	42
ΔT_j (°C)	10	29	20	13
N_f	2.064×10^{10}	2.827×10^{7}	2.917×10^{8}	2.917×10^{8}

The comparision analysis given in Table III show that the inverter 1 and inverter 3 take lower thermal stress than inverter 2 and inverter 4 under conventional droop control strategy. It can be seen that the equal thermal distributions are performed among four paralleled inverters under the proposed primary droop control. Lifetime of the microgrid can be evaluated according to the extended Coffin-Manson lifetime model (15). The number of cycles to failture (N_f) for inverter 2 and inverter 4 are obviously extended from 2.827×10^{7} to 2.917×10^{8}, which means that the mean lifetime of the microgrid is effectively improved.

With the development of power electronic technology, the wide bandgap semiconductors will be increasingly applied. To further validate the effectiveness of the proposed control method, simulation results are implemented in a SiC MOSFET-based microgrid. The parameters are given in Table IV.

TABLE IV

PARAMETERS APPLIED IN ELECTRO-THERMAL MODEL [38]-[39]

Inverter1/Inverter3		Inverter2/Inverter4	
SiC Power device	C3M0030090K	SiC Power device	C3M0065090J
R_{thJC_SiC}	0.62 K/w	R_{thJC_SiC}	1.1 K/w
R_{thHA_PD}	11 K/w	R_{thHA_PD}	11 K/w
Voltage (Base value)	110 V	Temperature (Base value)	75 °C
Current (Base value)	12 A	Frequency (Base value)	50 Hz

Fig. 15(a) shows the simulation result about thermal distribution among paralleled inverters under conventional droop control method. It can be seen that the thermal stress is unequally distributed due to difference of electro-thermal parameters for 4 inverters. Fig. 15(b) shows the simulation result under the proposed control method. It can be seen that the proposed control method is able to share automatically thermal stress. Hence, the simulation verification shows that the proposed control method is still effective in a SiC MOSFET-based microgrid.

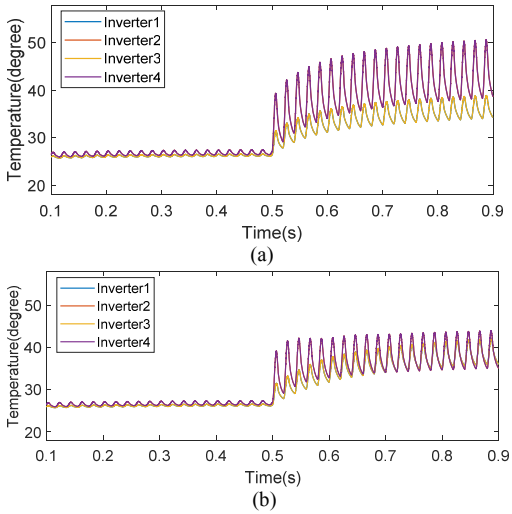

Fig. 15 The simulation results of the proposed control framework in a SiC MOSFET-based microgrid.

Case II Proposed secondary control strategy

Secondary control is proposed to optimize operation efficiency of microgrid. Fig. 16 shows simulation results about output power of paralleled inverters when system loads are decreased. It can be seen from Fig. 16(a) that the output powers of inverters are equally reduced when system loads are decreased at 0.2s. Fig. 16(b) shows that the operation efficiency of microgrid is decreased from 0.98 to 0.87.

Fig. 17 shows simulation results of microgrid with proposed secondary control strategy. It can be seen from Fig. 17(a) that the output powers of paralleled inverters are redistributed by optimizing number of inverters by secondary controller, where inverter 1 is controlled to generate more power, and the rest of inverters are reactivated. Fig. 17(b) shows overall efficiency curve of microgrid. It can be seen that the overall efficiency is improved once the proposed secondary control strategy is activated.

Fig. 18 shows simulation results of active thermal control. It can be seen that the average temperature is increased due to increase of load power at 0.2s. Once secondary controller is activated at 0.4s, active temperature control will be performed to decrease average temperature of inverters as shown in Fig.18(b).

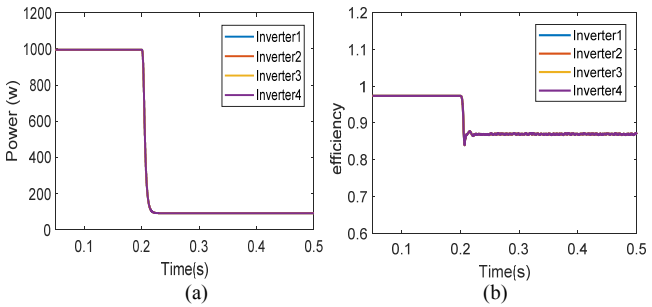

Fig. 16. Simulation results under conventional droop control strategy. (a) Output power of inverters. (b) Overall efficiency curve of inverters.

This article has been accepted for publication in a future issue of this journal, but has not been fully edited. Content may change prior to final publication. Citation information: DOI 10.1109/TEC.2020.3002670, IEEE Transactions on Energy Conversion

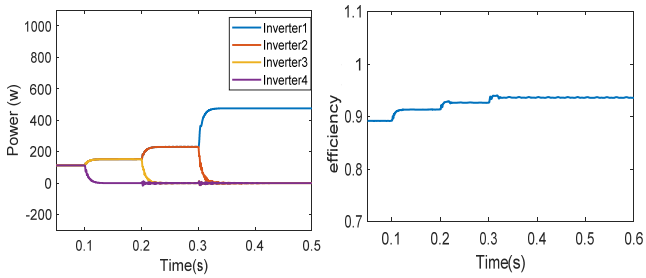

(a) (b)

Fig. 17. Simulation results about efficiency optimization mode under proposed secondary control strategy. (a) Output power of inverters. (b) Efficiency curve of inverter 1.

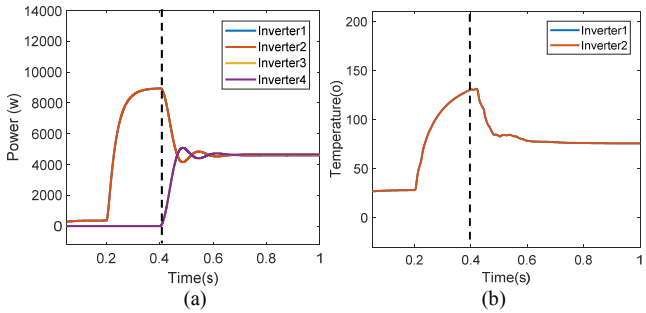

(a) (b)

Fig. 18. Simulation results with proposed secondary control strategy. (a) Output power of inverters. (b) Average temperature of inverters.

Fig. 19 shows simulation results of grid-connected microgrid with proposed secondary control strategy. It can be seen that resonance phenomenon is caused due to increase of grid impedance at 0.8s. The resonance phenomenon is mitigated once the proposed secondary control is activated at 1.1s, which agrees with the theoretical analysis results as shown in Fig. 9.

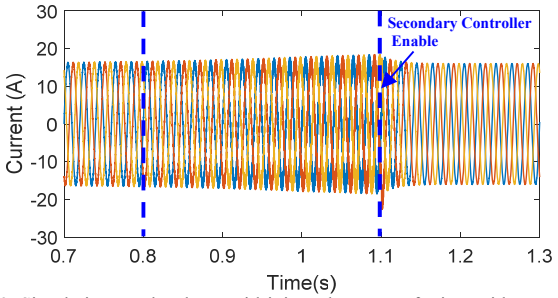

Fig. 19. Simulation results about grid-injected current of microgrid.

V. Experimental Verification

To further validate effectiveness of the proposed hierarchical control strategy, the experiments are implemented in a scaled-down microgrid with 3 inverters. The picture of experimental setup is shown in Fig. 18, where each inverter consists of three-phase bridge circuit, driving circuit of power modules, sampling circuit and *LC* filter. The circuit parameters applied in simulation and experiment are listed in Table III. The whole platform is controlled by dSPACE 1006.

TABLE V
SIMULATION AND EXPERIMENTAL PARAMETERS

Parameters	Value	Parameters	Value
f_s	10kHz	Phase Voltage (Simulation)	150 V
L_f	1.5mH	Phase Voltage (Experiment)	75 V
C_f	25μF	DC voltage (Simulation)	500V
L_c	2mH	DC voltage (Experiment)	200V
R_1/L_1	0.1Ω/2mH	R_2/L_2	0.1Ω/2mH

The proposed primary control strategy is first validated. Fig.20 shows experimental results under traditional droop control strategies. It can be seen from Fig. 20(a) that the output currents of paralleled inverters are increased to track change of load power, and output powers can be equally shared. Fig. 20(b) shows thermal imaging measurement results of inverter 1 and inverter 2. It can be seen that 6 power devices of inverter 1 become red color, which means the temperature of power devices is up to 89.9°C. Also, the thermal imaging of 6 power devices in inverter 2 shows grey color, which means the temperature of power devices is lower than 75°C. Hence, the thermal stresses of paralleled inverters are unequally distributed.

Fig. 21 shows experimental results of the proposed droop control strategies. It can be seen from Fig. 21(a) that the output currents of paralleled inverters are automatically adjusted to balance thermal stress of paralleled inverters. And Fig. 21(b) shows thermal imaging measurement results of inverter 1 and inverter 2. Thermal imaging of power devices in inverter 1 and inverter 2 shows almost same temperature profile, which means the temperature of power devices in two inverters are about 71°C. Hence, the thermal stresses of paralleled inverters are equally distributed under proposed droop control strategy.

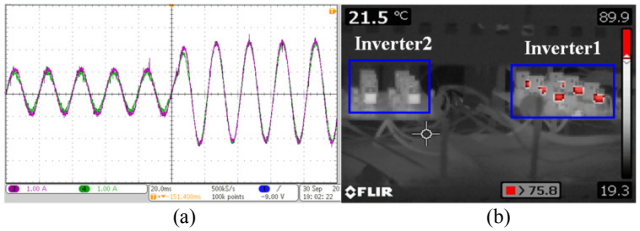

(a) (b)

Fig. 20. Experimental results under conventional droop control strategy. (a) Output currents (Phase A) of inverters. (b) Thermal stress distribution of inverters.

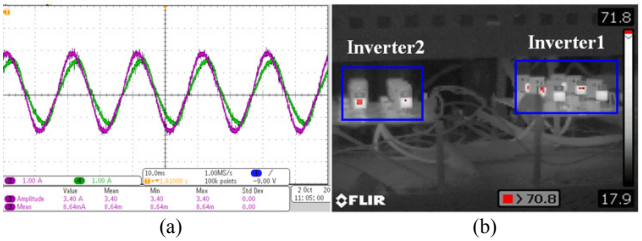

(a) (b)

Fig. 21. Experimental results under the proposed droop control strategy. (a) Output current (Phase A) of inverters. (b) Thermal stress distribution of inverters.

Fig. 22 show experimental results without proposed secondary control strategy, where the temperature of inverter 1 is up to 77.4°C as shown in Fig. 22(b). Once the secondary

control strategy is enabled, inverter 2 will be responsible for power sharing, then temperature is decreased to 42.3°C as shown in Fig. 23(b).

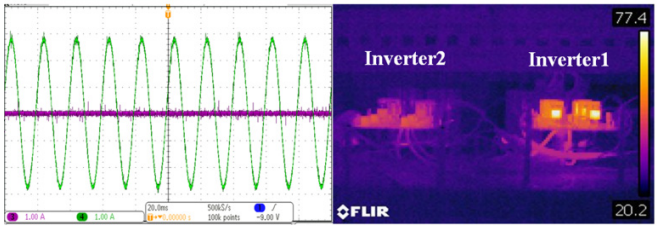

(a) (b)

Fig. 22. Experimental results without the proposed secondary control strategy. (a) Output current (Phase A) of inverters. (b) Thermal distribution of inverters.

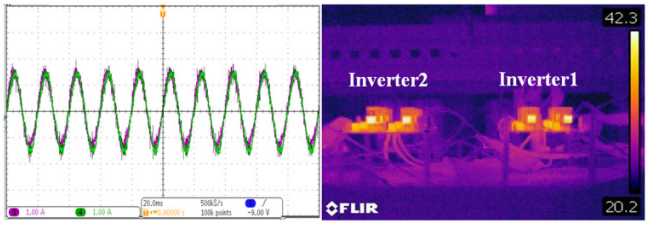

(a) (b)

Fig. 23. Experimental results with the proposed secondary control strategy. (a) Output current (Phase A) of inverters. (b) Thermal distribution of inverters.

In grid-connected mode, the microgrid with three 5kw inverters are established to validate the proposed secondary control strategy. Fig. 24(a) shows stable output currents of three DG inverters, which means the microgrid can be stably operated in a stiff grid. Once grid impedance is increased, resonance phenomenon of output currents can be caused as shown in Fig. 24(b). Then, the resonance phenomenon happens in the microgrid.

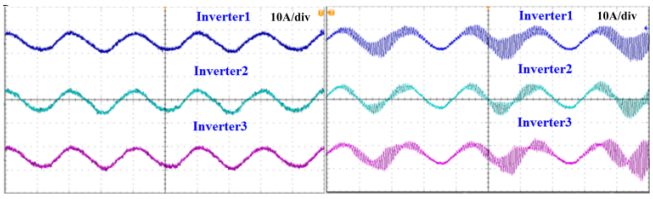

(a) (b)

Fig. 24. Experimental results of grid-connected microgrid. (a) Output currents (Phase A) of inverters in a stiff grid. (b) Output currents (Phase A) of inverters after the grid impedance is increased.

Fig. 25 shows experimental results about the proposed secondary control strategy. The resonance phenomenon of microgrid with two inverters can be seen as shown in Fig.25(a). It can be seen that once the proposed secondary control strategy shown in the Fig. 10 is activated, the resonance phenomenon can be mitigated as number decrease of inverters as shown in Fig. 25(b). Stable power is then transmitted into utility grid, which agrees with the theoretical analysis from Fig. 9 and simulation results as shown in Fig.19.

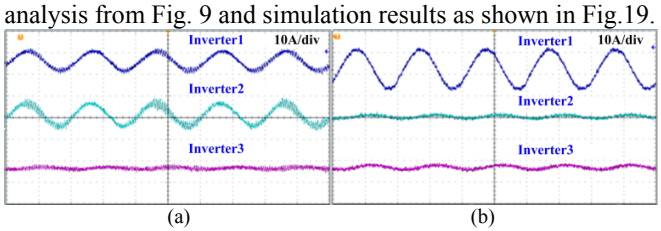

(a) (b)

Fig. 25. Experimental results of grid-connected microgrid. (a) Output currents (Phase A) of two inverters with proposed secondary control strategy. (b) Output current (Phase A) of one inverter with proposed secondary control strategy.

Therefore, the experimental results from Fig. 20-25 validate the proposed enhanced hierarchical control strategy.

VI. Conclusion

This paper presents an enhanced hierarchical control framework of microgrids with efficiency and reliability improvement. Primary control level is proposed to implement active thermal management. Secondary control level is developed to perform efficiency optimization and active thermal control according to different load profiles. In addition, resonance mitigation capability of microgrid is developed in this secondary control level. The simulation and experimental verification show that (1) The proposed primary control level is able to perform equal thermal distribution by regulating output powers of inverters. (2) Operation efficiency of microgrid under different load profiles can be improved by the proposed secondary control strategy. In addition, the proposed secondary control layer is able to mitigate resonance phenomenon in grid-connected mode. The proposed hierarchical control framework is able to enhance operation efficiency and perform active thermal management for microgrids. As a complementary, the proposed hierarchical control preserves inherent features of conventional hierarchical control.

Acknowledgment

The authors would like to thank for financial support from ForsKEL and EUDP project “Voltage control and protection for a grid towards 100% power electronics and cable network (COPE)” (No. 880063).

References

[1] Y. Wang, Z. Chen, X. Wang, Y. Tian, Y. Tan, C. Yang, "An estimator-based distributed voltage predictive control strategy for AC islanded microgrids." *IEEE Trans. Power Electron*., vol. 30, no. 7, pp. 3934-3951, July. 2015.

[2] W. Yuan, Y. Wang, X. Ge, X. Hou, and H. Han, “A unified distributed control strategy for hybrid cascaded-parallel microgrid,” *IEEE Trans. Energy Convers.*, vol. 34, no. 4, pp. 2029-2040, Dec. 2019.

[3] S. D. Manshadi, and M. E. Khodayar, “A hierarchical electricity market structure for the smart grid paradigm,” *IEEE Trans. Smart Grid*, vol. 7, no. 4, pp. 1866-1875, Jul. 2016.

[4] V. H. Bui, A. Hussain, and H. M. Kim, “A multiagent-based hierarchical energy management strategy for multi-microgrids considering adjustable power and demand response,” *IEEE Trans. Smart Grid*, vol. 9, no. 2, pp. 1323-1333, Mar. 2018.

[5] Y. A. I. Mohamed, and A. A. Radwan, “Hierarchical control system for robust microgrid operation and seamless mode transfer in active distribution systems,” *IEEE Trans. Smart Grid*., vol. 2, no. 2, pp. 352-362, Jun, 2011.

[6] C. J. J. Joseph, M. R. Zolghadri, A. Homaifa, F. C. Lee, and R. D. Lorenz, “A novel thermal based current sharing control of parallel converters”. in *Proc. 2004 26th Annual International Telecommunications Energy Conference*, 2004, pp. 647-653.

[7] Y. Wang, X. Wang, Z. Chen, and F. Blaabjerg, “ Distributed optimal control of reactive power and voltage in islanded microgrids,” *IEEE Trans. on Ind. Appl.*, vol. 53, no. 1, pp. 340-349, Jan. 2017.

[8] P. Liu, Y. Wang, J. Li, and D. Liu., “Advanced sensorless power control strategy of renewable microgrids for reliability enhancement”, *Applied Energy*, vol. 255, Dec. 2019.

[9] Y. Wang, D. Liu, P. Liu, F. Deng, D. Zhou, and Z. Chen, “Lifetime-oriented droop control strategy for AC islanded microgrids,” *IEEE Trans. Ind. Appl.*, vol. 55, no. 3, pp. 3252-3263, May/June, 2019.

[10] K. Ma, M. Liserre, F. Blaabjerg and T. Kerekes, "Thermal loading and lifetime estimation for power device considering mission profiles in

wind power converter." *IEEE Trans. Power Electron*., vol. 30, no. 2, pp. 590-602, Feb. 2015.

[11] M. Andresen, and M. Liserre, "Impact of active thermal management on power electronics design." *Microelectronics Reliability*, vol. 54, no. 9-10, pp. 1935-1939, Sep. 2014.

[12] M. Andresen, M. Liserre, and G. Buticchi, "Review of active thermal and lifetime control techniques for power electronic modules," *IEEE Trans. Power Electron.*, vol. 30, no. 3, pp. 1605-1617, Mar. 2015.

[13] M. Andresen, K. Ma, G. Buticchi, J. Falck, F. Blaabjerg and M. Liserre, "Junction Temperature Control for More Reliable Power Electronics," *IEEE Trans. Power Electron.*, vol. 33, no. 1, pp. 765-776, Jan. 2018.

[14] K. Ma and F. Blaabjerg, "Thermal optimised modulation methods of three-level neutral-point-clamped inverter for 10 MW wind turbines under low-voltage ride through," *IET Power Electronics*, vol. 5, no. 6, pp. 920-927, July. 2012.

[15] J. Lemmens, J. Driesen and P. Vanassche, "Dynamic DC-link voltage adaptation for thermal management of traction drives," *2013 IEEE Energy Conversion Congress and Exposition*, Denver, 2013, pp. 180-187.

[16] K. Ma, M. Liserre and F. Blaabjerg, "Reactive Power Influence on the Thermal Cycling of Multi-MW Wind Power Inverter," *IEEE Trans. on Ind. Appl.*, vol. 49, no. 2, pp. 922-930, Mar.-April. 2013.

[17] H. Luo, F. Iannuzzo, K. Ma, F. Blaabjerg, W. Li and X. He, "Active gate driving method for reliability improvement of IGBTs via junction temperature swing reduction," in *Proc. 2016 IEEE 7th International Symposium on Power Electronics for Distributed Generation Systems (PEDG)*, 2016, pp. 1-7.

[18] B. Wang, J. Cai, X. Du, and L. Zhou, "Review of power semiconductor device reliability for power converters," CPSS *Trans. Power Electron*., vol. 2, no. 2, pp. 101-117, Jun. 2017.

[19] M. Andresen, G. Buticchi, and M. Liserre, "Study of reliability-efficiency tradeoff of active thermal control for power electronic systems," *Microelectronics Reliability,* vol. 58, pp. 119-125, Mar. 2016.

[20] X. Yu, A. M. Khambadkone, H. Wang, and S. T. S. Terence. "Control of parallel connected power converters for low voltage microgrid—Part I: A hybrid control architecture." *IEEE Trans. Power Electron*., vol. 25, no. 12, pp. 2962-2970, Dec. 2010.

[21] H. Wang, A. M. Khambadkone, and X. Yu. "Control of parallel connected power converters for low voltage microgrid—Part II: Dynamic electro-thermal modeling." *IEEE Trans. Power Electron*. vol. 25, no. 12, pp. 2971-2980, Dec. 2010.

[22] L. Meng, T. Dragicevic, J. M. Guerrero, and J. C. Vasquez, "Dynamic consensus algorithm based distributed global efficiency optimization of a droop controlled DC microgrid," in *Proc. Energycon*, May 13-16, 2014, pp. 1-8.

[23] W. Yuan, Y. Wang, D. Liu, F. Deng, and Z. Chen, "Efficiency-prioritized droop control strategy of AC microgrid," *IEEE J. Emerg. Sel. Topics Power Electron*., (early access), 2020. Doi: 10.1109/JESTPE.2020.2967756

[24] W. Yuan, Y. Wang, D. Liu, and F. Deng, "Adaptive droop control strategy of autonomous microgrid for efficiency improvement," in *Proc. 2019 IEEE 7th International Symposium on Power Electronics for Distributed Generation Systems (PEDG)*, Jun 3-6, 2019. pp. 972-977.

[25] Y. Wang, X. Wang, F. Blaabjerg, and Z. Chen, "Harmonic instability assessment using state-space modeling and participation analysis in inverter-fed power systems," *IEEE Trans. Ind. Electron*., vol. 64, no. 1, pp. 806-816, Jan, 2017.

[26] J. Sun, "Impedance-based stability criterion for grid-connected inverters," *IEEE Trans. Power Electron.,* vol. 26, no. 11, pp. 3075-3078, Nov. 2011.

[27] X. Wang, F. Blaabjerg, and W. Wu, "Modeling and analysis of harmonic stability in an AC power-electronics-based power system," *IEEE Trans. Power Electron.*, vol. 29, no. 7, Jul, 2015.

[28] Y. Wang, X. Wang, F. Blaabjerg, and Z. Chen, "Harmonic resonance assessment of multiple paralleled grid-connected inverters system," in *Proc. 2017 IEEE Future Energy Electronics Conference and ECCE Asia (IFEEC-ECCE Asia)*, pp. 2070–2075.

[29] Y. Wang, D. Liu, Z. Chen and P. Liu, "A hierarchical control strategy of microgrids toward reliability enhancement,'' in *Proc.6th IEEE International Conference on Smart Grid,* 2018, pp. 123-128.

[30] S. Rohner, S. Bernet, M. Hiller, and R. Sommer, "Modulation, losses, and semiconductor requirements of modular multilevel converters." *IEEE Trans. on Ind. Electron*., vol. 57, no. 8, pp. 2633-2642, Aug. 2010.

[31] Infineon Technical Documentation. "Dimensioning program IPOSIM for loss and thermal calculation of infineon IGBT modules."

[32] Y. Yang, H. Wang, F. Blaabjerg and K. Ma, "Mission profile based multi-disciplinary analysis of power modules in single-phase transformerless photovoltaic inverters," in *Proc. 2013 15th European Conference on Power Electronics and Applications (EPE)*, Lille, 2013, pp. 1-10.

[33] "IGBT modules technical information," FS6R06VE3_B2, Infineon datasheet, 2007.

[34] "IGBTmodules technical information," FP10R06KL4, Infineon datasheet, 2007.

[35] https://www.ohmite.com/assets/docs/sink_w.pdf?r=false

[36] D. Zhou, F. Blaabjerg, T. Franke, M. Tønnes, and M. Lau,, "Comparison of wind power converter reliability with low-speed and medioum-speed permanent-magnet synchronous generators," *IEEE Trans. on Ind. Electron*., vol. 62, no. 10, pp. 6575-6584, Oct. 2015.

[37] D. Lee, and M. Yannakakis, "Principles and methods of testing finite state machines – A survey." *Proceedings of the IEEE*, vol. 84, no. 8, pp. 1090-1123, Aug. 1996.

[38] CREE C3M0030090K Silicon Carbide Power MOSFET Datasheet.https://www.wolfspeed.com/media/downloads/1185/C3M0030090K.pdf

[39] CREE C3M0030090J Silicon Carbide Power MOSFET Datasheet.https://www.wolfspeed.com/media/downloads/145/C3M0065090J.pdf